Journal of Power Sources 255 (2014) 37–42

Contents lists available at ScienceDirect

Journal of Power Sources

journal homepage: www.elsevier.com/locate/jpowsour

Short communication

Graphene/Au composite paper as flexible current collector to improve electrochemical performances of CF_x cathode

Weijing Yang [a,b,1], Yang Dai [a,b,1], Sendan Cai [a,b], Yi Zheng [a], Wen Wen [c], Ke Wang [a,b], Yi Feng [a], Jingying Xie [a,b,*]

[a] Shanghai Institute of Space Power Sources, Shanghai 200245, China
[b] Shanghai Engineering Center for Power and Energy Storage Systems, Shanghai 200245, China
[c] BL14B1 Shanghai Synchrotron Radiation Facility, Shanghai 201204, China

HIGHLIGHTS

- Graphene/Au composite paper was use as a current collector for CF_x cathode.
- The rate performances of the CF_x cathodes can be greatly improved.
- Maximum power density of 8000 W kg^{-1} at 5C rate can be achieved with $CF_{1.0}$.
- Provide a new strategy to design both high power and energy densities CF_x cathode.

ARTICLE INFO

Article history:
Received 22 August 2013
Received in revised form
21 December 2013
Accepted 29 December 2013
Available online 4 January 2014

Keywords:
Graphene/Au composite paper
Interface
Current collector
Rate performance
CF_x battery

ABSTRACT

We report the application of free-standing, lightweight, and flexible graphene/Au composite paper (GACP), as a current collector for CF_x cathode. At a high discharge current density of 4000 mA g^{-1} (5C), the capacity of the $CF_{1.0}$ loaded on GACP current collector is 653 mAh g^{-1}, while $CF_{1.0}$ loaded on Al foil failed at 800 mA g^{-1} (1C). Using GACP, both excellent rate capability and specific capacity can be achieved simultaneously, owing to its undulant surface structure and flexible contact with the CF_x composite active layer. Our results provide a new strategy to design both high power and energy densities CF_x cathode.

1. Introduction

CF_x battery possesses the highest energy density among all primary lithium batteries with a theoretical value of 2180 Wh kg^{-1}, presenting several advantages of high and flat discharge potential (about 2.5–2.8 V), large temperature range of use (from −40 °C to 170 °C), long shelf life (7–10 years), and so on. So it is of great interest as portable energy storage devices in electronics, medical implants, and space applications. The first use of CF_x as the active cathode material in primary lithium battery was reported by Watanabe and Fukuda and then a few years later, the first Li/$CF_{1.0}$ batteries were commercialized by Matsushita Electric Co. in Japan [1–3]. Since then, many fluorinated methods and electrochemical behaviors of fluorinated carbon have been widely investigated [3–11] in the earlier ages. And the possible mechanisms have been established [11–15]. Unfortunately, the battery is still known to suffer from kinetic problems due to the cathode material CF_x is intrinsically a poor electronic conductor, inhibiting its application in high-power devices [3,16–18]. So recently, considerable effort is being devoted to address these problems. A large quantity of reports focuses on the cathode materials improvement. Therefore, various fluorinated methods and nanoscale fluorinated carbon were developed. Making the CF_x conductive by decreasing the fluorine content to form sub-fluorinated carbons is an effective way [19]. Other approaches were devoted to the conducting network optimization, such as conductive carbon selecting [20], and taking

* Corresponding author. Shanghai Institute of Space Power Sources, Shanghai 200245, China.
E-mail address: jyxie@mail.sim.ac.cn (J. Xie).
[1] These authors contributed equally to this article.

0378-7753/$ – see front matter
http://dx.doi.org/10.1016/j.jpowsour.2013.12.122

advantage of the synergistic effect by mixing with metal oxides [12,16,17]. Recently, P. Meduri et al. [16] show good electrochemical performances of the hybrid carbon fluoride (CF_x)/silver vanadium oxide (SVO)/graphene cathode, with specific capacity of around 462 mAh g^{-1} at 5C rate. However, while the methods mentioned above improve the rate capability, a great part of capacity is lost.

Herein, we report a new method to improve the rate capability without compromising the capacity of the CF_x electrode by simply applying the graphene/Au composite paper as a current collector. Most researchers paid less attention to the current collector's effect on CF_x cathodes before. CF_x materials with two different fluorine contents ($x = 0.8$ and $x = 1$) are used to evaluate. The results demonstrate the electrochemical performances using GACP current collector can be greatly improved.

2. Experimental

A detailed description of the Graphene/Au composite paper preparing procedure is described elsewhere [8]. Briefly, A mixed aqueous solution (200 mL), which contains GO (1 mg mL^{-1}), ascorbic acid (10 mg mL^{-1}) and $HAuCl_4$ (0.25 mg L^{-1}), was first treated by ultrasonication (40 kHz, 600 W) for 0.5 h. Then the mixture was heated and maintained at 90 °C for 45 min. The aqueous dispersion was then filtered to form graphene/noble metal composite paper. The as prepared paper was annealed in the atmosphere of Ar 8 v/v% H_2 at 300 °C for 3 h and then pressed with a pressure of 10 MPa. The electrical conductivity of the resultant graphene paper was determined using an SX1944 four point probe meter (Suzhou 126 Telecommunication Instrument), with a conductivity of 9340 S m^{-1}.

The gray $CF_{0.8}$ and white $CF_{1.0}$ powder were purchased from Fubang Shanghai and donated by Daikin Japan, respectively. CF_x (80 wt%) powder, PVDF resin (10 wt%, Kynar 761), and vapor grown carbon fiber (VGCF, 10%, Showa Denko Co.) were mixed and stirred vigorously in the presence of N-methyl-2-pyrrolidone to form a uniform slurry. The cathodes were prepared by spreading the same slurry onto aluminum foil (18 μm, Alcoa.) and graphene paper based (12 μm after pressed) current collectors. The thickness of the composite active layers is set around 25 μm after dried and pressed. Then the paper and Al foil with composite active layer were punched into 1.4 cm in diameter disks, whose active mass loading were 1–1.5 mg cm^{-2}.

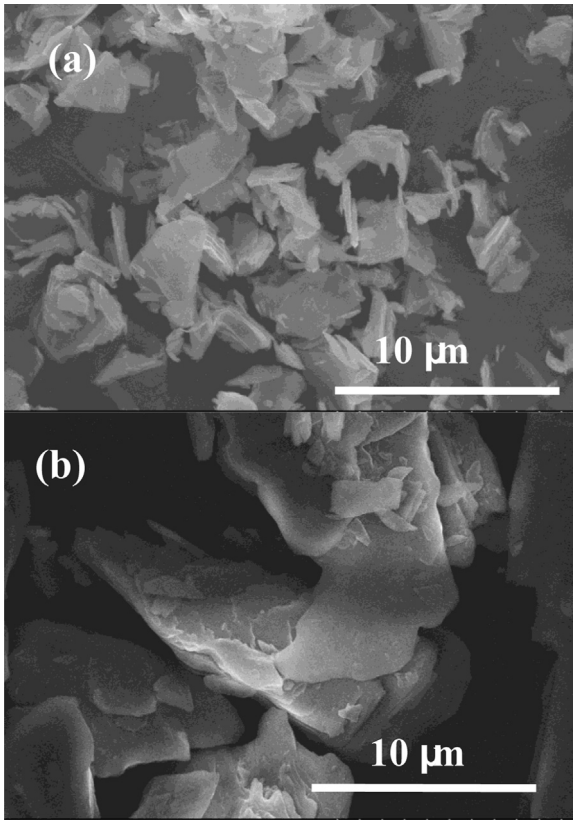

Fig. 1. SEM images of the cathode materials (a) $CF_{0.8}$ and (b) $CF_{1.0}$. The scale bars are both 10 μm.

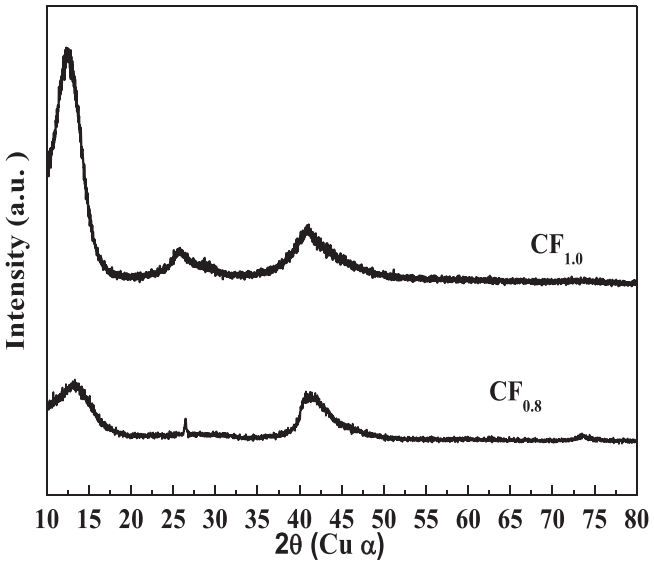

Fig. 2. XRD patterns of the cathode materials $CF_{0.8}$ and $CF_{1.0}$.

3. Results and discussion

The colors of the $CF_{0.8}$ and $CF_{1.0}$ are dark gray and white-gray, indicating the different fluorinated content. Fig. 1 exhibits the SEM images of the two kinds of the CF_x. The images show the typical layer stacking structure and morphology of the $CF_{0.8}$ and $CF_{1.0}$, indicating the both CF_x may be made from graphite-like precursor. The particle size of the $CF_{0.8}$ 3–5 μm, while the $CF_{1.0}$ is 10–15 μm. The blur edge of the $CF_{1.0}$ particle suggests the more poor electrical

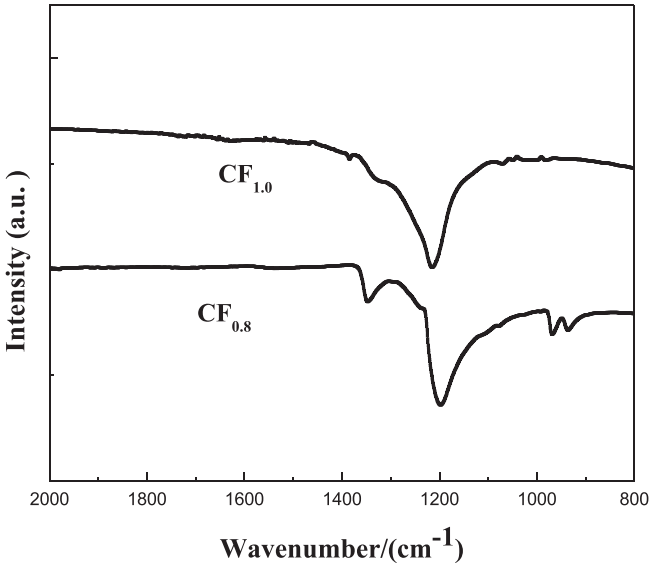

Fig. 3. FTIR spectra of the cathode materials $CF_{0.8}$ and $CF_{1.0}$.

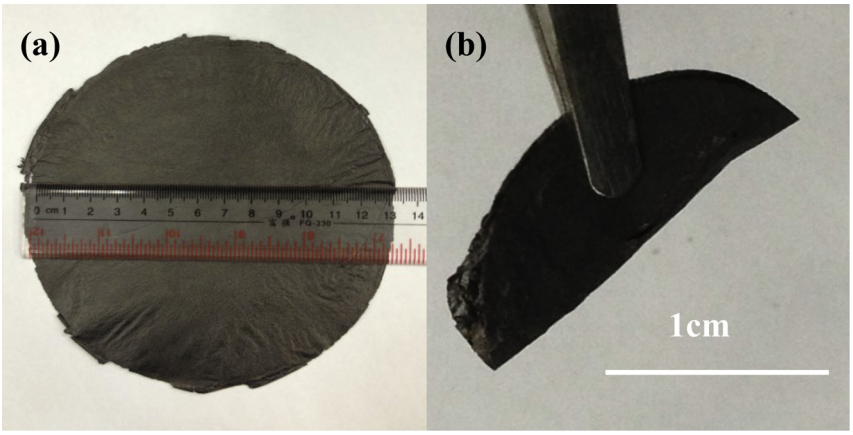

Fig. 4. (a) Graphene/Au composite paper after annealed, with a diameter of 13 cm. (b) Photograph of the doubled up $CF_{1.0}$ cathode using GACP based current collector, indicates the flexibility of the electrode. The scale bar is 1 cm.

conductivity, which may origin from the highly fluorination. The XRD patterns are shown in Fig. 2. The typical broad peaks corresponding to the fluorinated phases ($2\theta \approx 13°$, 26°and 41°) are indicated in the both spectra. The peak around 13° could be indexed in a hexagonal system either as the 001 reflection or as a 002 reflection [3]. The reflection corresponds to average interlayer spacing. The interlayer spacing of the $CF_{0.8}$ and $CF_{1.0}$ are 6.7 Å and 7.1 Å, respectively. And from the FTIR spectra (Fig. 3), the both CF_x exhibit an intense band centered at around 1214 cm^{-1}, which is the characteristic band of the covalent C—F bond [3]. The bands at 1342 and 1072 cm^{-1}, have been assigned to the asymmetric and symmetric stretching vibration of $>CF_2$ groups at the edge of the graphite layers. From the spectra, the two bands appear in the $CF_{0.8}$ and $CF_{1.0}$ materials, suggesting the both materials contain $>CF_2$ groups.

The photo of the annealed Au/graphene composite paper with a diameter of 13 cm is exhibited in Fig. 4(a). Fig. 4(b) presents the photograph of $CF_{1.0}$ cathode using GACP current collector, which can be doubled up without any crease, revealing the flexibility and durability of the electrode. Small amount of Au is added in order to improve the mechanical durability and conductivity of the graphene paper. In addition, the Au nano particles will prevent the graphene layers from restacking during annealing. It should be noted that the weight of the GACP is only 1/8 that of the Al foil on equal area. More importantly, the GACP presents stability at the potential of 3–1.5 V. Lithium ions will not intercalate into the bare graphene/Au composite paper above 1.5 V vs. Li^+/Li (Fig. 5). The result verifies the feasibility of using GACP as the current collector for CF_x cathode.

Fig. 6 show the SEM images of the bared Al foil and GACP current collectors. Compared to the Al foil, the graphene paper exhibits rough and crinkled surface, which may be favorable for the composite active layer adhesion [21]. The cross-section SEM image of the graphene paper based electrode (inset of Fig. 6(b)), indicates the undulating morphology of the GACP based current collector,

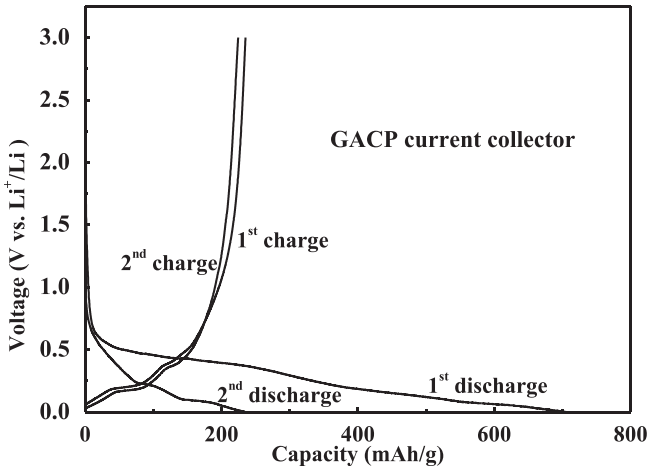

Fig. 5. (a) Charge–discharge curves of GACP bare electrode, with a current density of 20 mA g^{-1} (0–3 V).

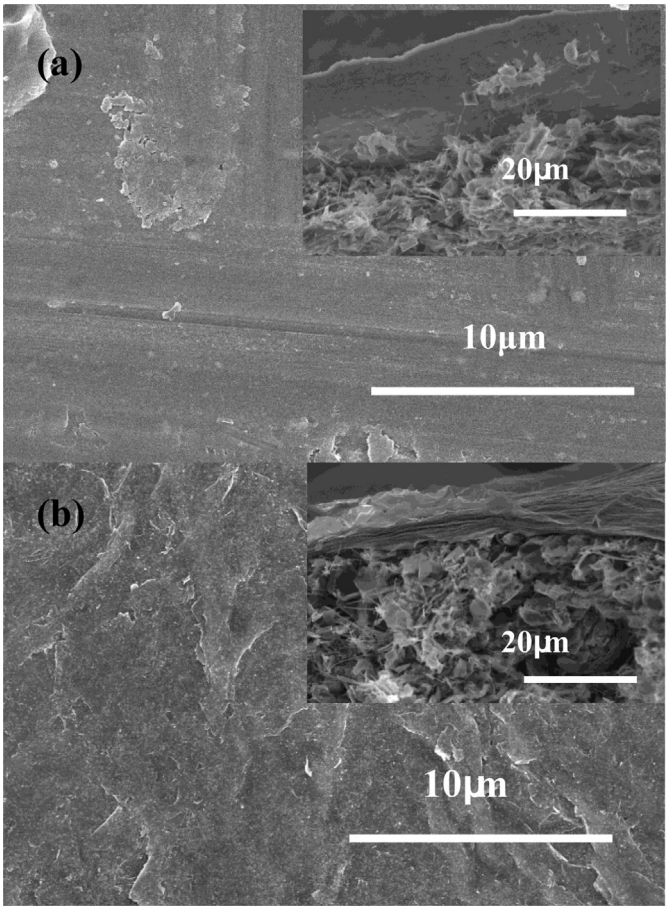

Fig. 6. (a) The SEM images of the bare and Al foil (b) and GACP current collectors. The inset pictures are cross-sectional SEM of the $CF_{0.8}$ electrodes using the correspondent current collectors. The scale bars are 10 μm for (a), (b), and 20 μm for inset images.

which can be considered as the flexible contact with the active layer compared to the rigid contact of the Al foil based current collector (inset of Fig. 6(a)). The flexible substrate will abate the stress caused by swelling of the CF_x during discharge.

The rate performances of the $CF_{0.8}$ and $CF_{1.0}$ cathodes using Al foil and GACP based current collectors are shown in Fig. 7. For the $CF_{0.8}$ cathodes (Fig. 7(a) and (b)), both the electrodes deliver a similar specific capacity of 760–770 mAh g^{-1}, with $E_{1/2}$ (the voltage at half of the total discharge) of 2.4 V. However, with the discharge current density increasing, the $E_{1/2}$ of the Al foil based electrode sharply decreases to 1.8 V at 1C. Severe voltage delays with "zigzag" discharge curves can be observed above 0.5C. In contrast, the graphene paper based electrode exhibits more well-defined curvatures of the all discharge curves and reduces voltage delays. The cathode can exert a capacity of 613 mAh g^{-1}, with a high power density of 7320 W kg^{-1}, even at 5C rate. The high capacity retention 5C/0.025C of 83%, indicates most of the active materials can be utilized at high current density. In the case of $CF_{1.0}$, the electrochemical performances are more contrasting (Fig. 7(c) and (d)). Using the Al foil current collector, the $CF_{1.0}$ cathode shows very badly-defined curve even at the low rate of 0.5C and is impossible to discharge at 1C, revealing a worse electrochemical performance compared to that of $CF_{0.8}$. While employing the GACP current collectors, the $CF_{1.0}$ cathodes present well-defined curves from 0.025C to 5C. Even at the high rate of 5C, a very high power density of 8000 W kg^{-1} can be obtained, with a capacity retention 5C/0.025C of 82%. It is interesting that the power density of $CF_{1.0}$ is even better than that of $CF_{0.8}$ at high rate using the GACP. The properties of the CF_x material itself, such as the electron and ion conductivity, interlayer spacing, grain size, and surface group contents (–CF_2, and –CF_3), will partially affect the rate capability. In this case, a larger interlayer spacing of $CF_{1.0}$ (7.1 Å compared to 6.7 Å of $CF_{0.8}$) may be favorable for lithium intercalation at high rate once the electron transfer is high enough. The reason is not so clear, and much work needs to be carried out to clarify. However, the results clearly demonstrate the paramount role of current collector in spite of what kind of CF_x. The superiority would be originated by the surface roughness and flexible adhesion to the composite active layer [21].

To better understand our findings, an AC impedance analysis at the open circuit voltage (OCV) of un-discharged cells was investigated. The Nyquist plots for impedance of different current collectors based electrodes are presented in Fig. 8(a) for $CF_{0.8}$, and Fig. 8(b) for $CF_{1.0}$. Both impedance spectra show suppressed semicircles followed by a slopping straight line at the lower frequency end. The real axis intercepts in the higher frequency region can be assigned to the bulk resistance (R_b) that generally includes the resistances of the current collector, electrode, separator and electrolyte. The semi-circle could be assigned to the cell reaction resistance (R_c), reflecting charge transfer resistance and the composite active layer/current collector interfacial resistances [22]. The insert picture, the R_b values of the cells are almost the same with the same kind of CF_x, indicating the difference of the current collector contributes little to the R_b. The impressive difference is that the graphene paper based cells has much lower R_c than the Al foil based cells, revealing the important part played by interfacial resistances.

Fig. 9(a) and (b) exhibit the digital pictures of $CF_{0.8}$ and $CF_{1.0}$ with different current collectors after discharge. The inset SEM images below are correspondent cross-sectional images. The plane-viewed SEM images of $CF_{0.8}$ electrode after discharge at 1C and $CF_{1.0}$ after discharge at 0.5C with different current collectors are indicated in Fig. 9(c)–(f). After discharge, small particles were generated and distributed on the surface of the electrodes to form surface

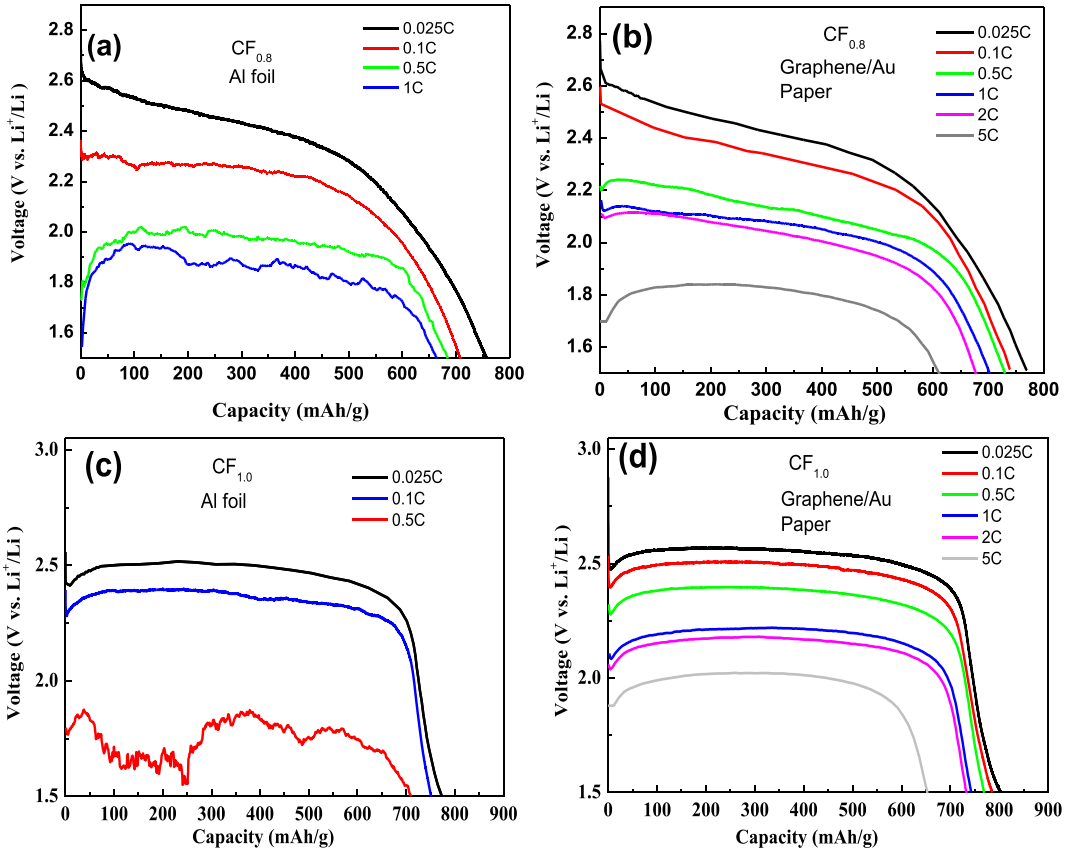

Fig. 7. Discharge profiles at different current densities of (a) Al foil based $CF_{0.8}$ cell, (b) GACP based $CF_{0.8}$ cell. (c) Al foil based $CF_{1.0}$ cell, (d) GACP based $CF_{1.0}$ cell.

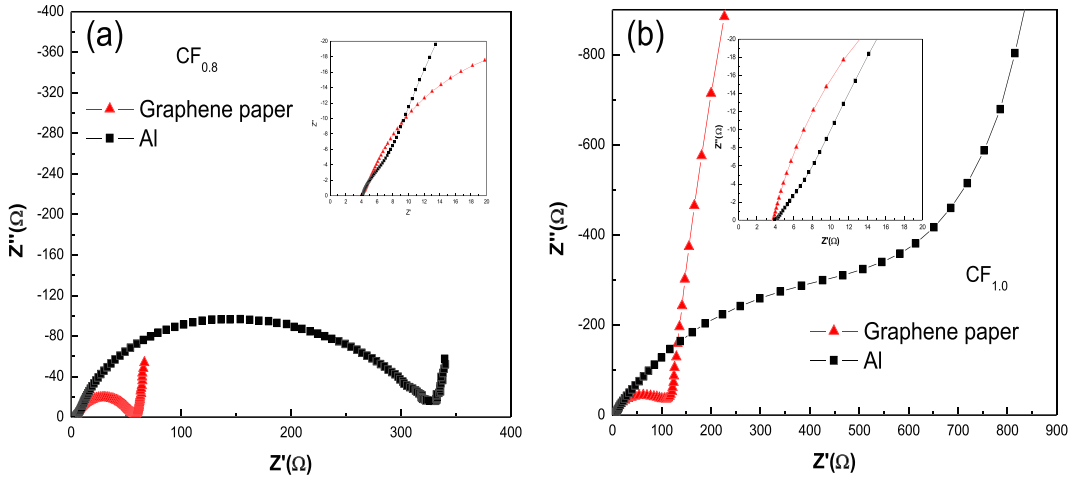

Fig. 8. AC impedance spectra of un-discharged cells measured at OCV for (a) $CF_{0.8}$ cell and (b) $CF_{1.0}$ cell with different current collectors.

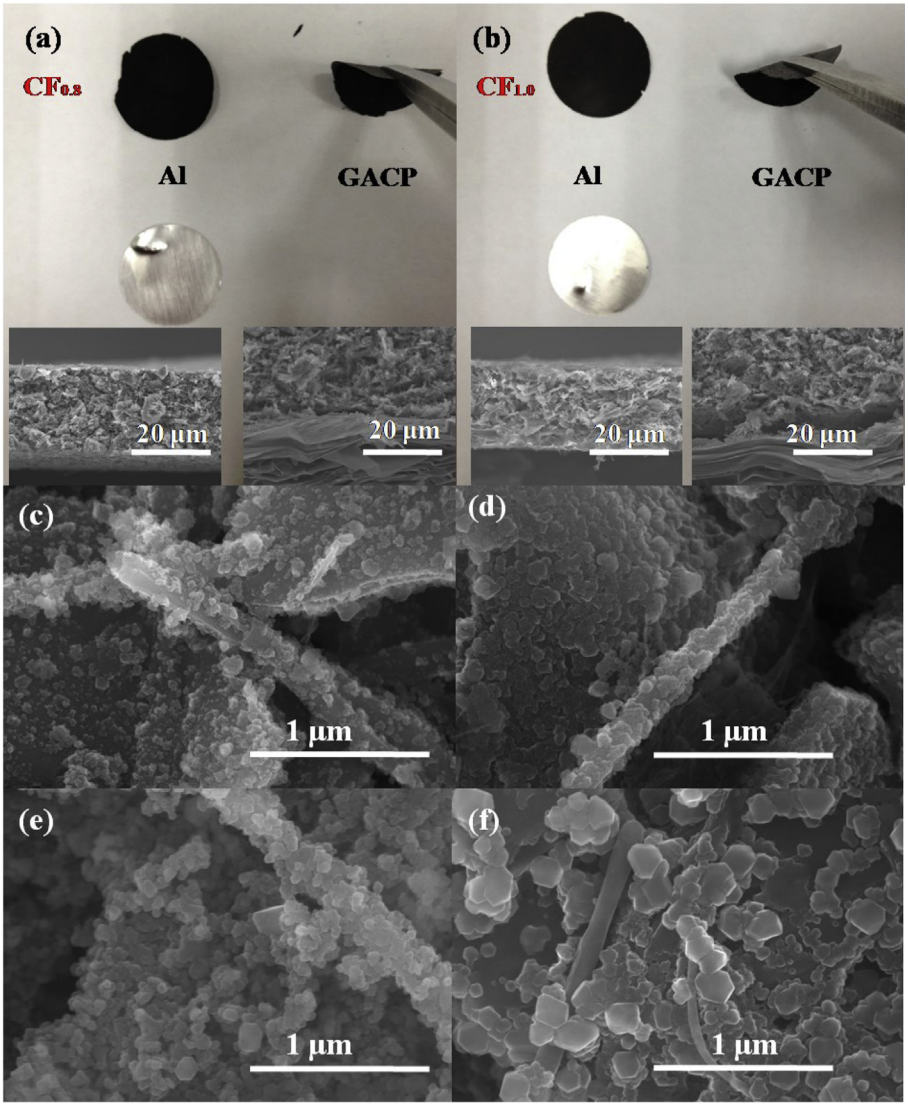

Fig. 9. Digital pictures of the electrodes after discharge (a) $CF_{0.8}$ with Al foil based (left part) and GACP based (right part) and (b) $CF_{1.0}$ with Al foil based (left part) and GACP based (right part), the inset SEM images below are correspondent cross-sectional images. The scale bars of the SEM images are all 20 μm. The plane-viewed SEM images of the (c) Al foil based $CF_{0.8}$ and (d) GACP based $CF_{0.8}$ electrodes after discharge at 1C, (e) Al foil based $CF_{1.0}$ and (f) GACP based $CF_{1.0}$ electrodes after discharge at 0.5C. The scale bar of the four images are all 1 μm.

layers. The small particles can be assigned to the LiF [23]. The particle size and shape are verified with different CF_x and current collectors. However, it needs further studies to reveal the mechanism. It can be clearly seen from the pictures and the cross-sectional SEM images (Fig. 9(a) and (b)) that the composite active layers are totally separated from the Al foils. In contrast, both the GACP based electrodes ($CF_{0.8}$ and $CF_{1.0}$) show the well adhered composite active layers to the current collectors even bending the electrodes. The results suggest the current collector play a paramount role in the electrode during the discharge process. The stress arising from the CF_x composite layer swelling during discharge could be ascribed to this exfoliation. The swelling is common in CF_x cathode, which may be due to the formation of volumetric LiF crystals during discharge [14,15,22,24].

A widely accepted reaction of Li/CF_x cell can be described as [12–15]:

$$\text{Anode}: xLi + xS \rightarrow xLi^+S + xe \quad (1)$$

$$\text{Cathode}: CF_x + xLi^+S + xe \rightarrow C\left(Li^+S - F^-\right)_x \quad (2)$$

$$C\left(Li^+S - F^-\right)_x \rightarrow C + xLiF + xS \quad (3)$$

$$\text{Total}: \quad xLi + CFx \rightarrow C + xLiF \quad (4)$$

where S represents one or more solvent molecules coordinated with each Li^+ ion and C ($Li^+S{-}F^-$) the graphite intercalation compound (GIC) intermediate that subsequently decomposes into the final discharge products, carbon and lithium fluoride (LiF). Three steps are involved in the discharge reaction: (1) the transport of solvated lithium ions into F-graphene layers, (2) the formation of GIC intermediate and (3) the transfer of electrons from current collector to CF_x and the dissociation of GIC intermediate. The mechanism above has shown that the main slow transport of solvated lithium ions in the GIC intermediate layer is the controlling step in cathode reaction. It seems the step (3) is not a problem under an idea condition. However, the discharge of the cathode is accompanied by significant swelling due to the formation of volumetric LiF crystals. And the stress between the composite active layer and the current collector will generate. The stress may cause the partial separation of the composite active layer from the rigid Al current collector, leading to blocking the electron transfer. So the noisy curves of rigid Al foil based cells at higher discharge rate may be due to the loss of contact with the rigid current collectors. To the contrary, the flexible GACP substrate may be beneficial to abate the stress caused by CF_x swelling. That keeps well contact with the composite active layer, guaranteeing the transfer of electron.

4. Conclusion

Graphene/Au composite paper was applied as a novel current collector to improve the rate performances without compromising the high capacity. High specific capacity of 653 mAh g^{-1} and maximum power density of 8000 W kg^{-1} at 5C rate can be achieved with $CF_{1.0}$. The superiority of the flexible GACP based current collector, could be originated by the rough surface and flexible carbon–carbon contact to the active layer, which favors the interfacial electron transfer. Our finding here stresses the paramount role of composite active layer/current collector interface, providing a new strategy to design both high power and energy densities CF_x cathode. Furthermore, the method is independent on the active materials and therefore may apply for other lithium chemistries.

Acknowledgments

This work was supported by National Natural Science Foundation of China (No. 21103109, No. 21373137), National 863 Program (No. 2013AA050902), Shanghai Science and Technology Talent Program (No. 12XD1421900). The beamlines BL14B1 and BL08U1A, at the Shanghai Synchrotron Radiation Facility (SSRF) (Shanghai, China) are appreciated.

References

[1] N. Watanabe, M. Fukuda, US Patent 3,536,532 (1970) and 3,700,502(1972).
[2] M. Fukuda, T. Iijima, in: D.H. Collins (Ed.), Power Sources, 5, Academic Press, New York, 1975, p. 713.
[3] K. Guerin, M. Dubois, A. Houdayer, A. Hamwi, J. Fluorine Chem. 134 (2012) 11.
[4] N. Watanabe, T. Nakajima, H. Touhara, Graphite Fluorides, Elsevier, Amsterdam, 1988.
[5] A. Hamwi, K. Guerin, M. Dubois, Fluorinated Materials for Energy Conversion, Elsevier, Oxford, UK, 2005.
[6] I. Palchan, D. Davidov, H. Selig, J. Chem. Soc. Chem. Commun. 12 (1983) 657.
[7] T. Nakajima, N. Watanabe, I. Kameda, M. Endo, Carbon 24 (1986) 343.
[8] A. Hamwi, M. Daoud, J.C. Cousseins, Synth. Met. 26 (1988) 89.
[9] K. Gue rin, J.P. Pinheiro, M. Dubois, Z. Fawal, F. Masin, R. Yazami, A. Hamwi, Chem. Mater. 16 (2004) 1786.
[10] K. Guerin, R. Yazami, A. Hamwi, Electrochem. Solid State Lett. 7 (6) (2004) A159.
[11] R. Hagiwara, T. Nakajima, N. Watanabe, J. Electrochem. Soc. 135 (9) (1988) 2128.
[12] S. Zhang, D. Foster, J. Read, J. Power Sources 18 (2009) 601.
[13] Q. Zhang, S. D'Astorga, P. Xiao, X. Zhang, L. Lu, J. Power Sources 195 (2010) 2914.
[14] N. Watanabe, R. Hagiwara, T. Nakajima, H. Touhara, K. Ueno, Electrochim. Acta 27 (1982) 1615–1619.
[15] N. Watanabe, T. Nakajima, R. Hagiwara, J. Power Sources 20 (1987) 87–92.
[16] P. Meduri, H. Chen, X. Chen, J. Xiao, M. Gross, T. Carlson, J. Zhang, Z. Deng, Electrochem. Commun. 13 (2011) 1344.
[17] H. Groult, C.M. Julien, A. Bahloul, S. Leclerc, E. Briot, A. Mauger, Electrochem. Commun. 13 (2011) 1074.
[18] M. Duboisa, K. Guérina, W. Zhang, Y. Ahmad, A. Hamwi, Z. Fawal, H. Kharbache, F. Masin, Electrochim. Acta 59 (2012) 485.
[19] P. Lam, R. Yazami, J. Power Sources 153 (2006) 354.
[20] Y. Li, Y. Chen, W. Feng, F. Ding, X. Liu, J. Power Sources 196 (2011) 2246.
[21] Y. Dai, S. Cai, W. Yang, L. Gao, W. Tang, J. Xie, J. Zhi, X. Ju, Carbon 50 (2012) 4648.
[22] S. Yoshihara, H. Isozumi, M. Kasai, H. Yonehara, Y. Ando, K. Oyaizu, H. Nishide, J. Phys. Chem. B 114 (2010) 8335.
[23] J. Read, E. Collins, B. Piekarski, S. Zhang, J. Electrochem. Soc. 158 (2011) A504.
[24] S. Zhang, D. Foster, J. Read, J. Power Sources 18 (2009) 233.